TU Delft

Delft University of Technology

Document Version
Final published version

Licence
CC BY

Citation (APA)
Yibole, H., Shanshan, L., Narsu, B., Guillou, F., Detlefs, B., Glatzel, P., Hanggai, W., Kiecana, A., Van Dijk, N. H., & Brück, E. (2026). Magnetic moments evolution in $(Mn,Fe)_2(P,Si)$ single crystals from x-ray emission spectroscopy. *Physical Review Materials*, *10*(3), Article 034412. https://doi.org/10.1103/dzwg-bnpp

Important note
To cite this publication, please use the final published version (if applicable).
Please check the document version above.

Copyright
In case the licence states “Dutch Copyright Act (Article 25fa)”, this publication was made available Green Open Access via the TU Delft Institutional Repository pursuant to Dutch Copyright Act (Article 25fa, the Taverne amendment). This provision does not affect copyright ownership.
Unless copyright is transferred by contract or statute, it remains with the copyright holder.

Sharing and reuse
Other than for strictly personal use, it is not permitted to download, forward or distribute the text or part of it, without the consent of the author(s) and/or copyright holder(s), unless the work is under an open content license such as Creative Commons.

Takedown policy
Please contact us and provide details if you believe this document breaches copyrights.
We will remove access to the work immediately and investigate your claim.

This work is downloaded from Delft University of Technology.

Magnetic moments evolution in $(Mn,Fe)_2(P,Si)$ single crystals from x-ray emission spectroscopy

H. Yibole,[1] L. Shanshan,[1] B. Narsu,[1] F. Guillou,[1,2,*] B. Detlefs,[3] P. Glatzel,[3] W. Hanggai,[4] A. Kiecana,[4] N. H. van Dijk,[4] and E. Brück[4]

[1]*College of Physics and Electronic Information, Inner Mongolia Key Laboratory of Applied Condensed Matter Physics, Inner Mongolia Normal University, 81 Zhaowuda Rd., Hohhot 010022, China*

[2]*Normandie Univ., ENSICAEN, UNICAEN, CNRS, CRISMAT, 14000 Caen, France*

[3]*European Synchrotron Radiation Facility, 38000 Grenoble, France*

[4]*Fundamental Aspects of Materials and Energy (FAME), Faculty of Applied Sciences, Delft University of Technology, Mekelweg 15, 2629JB Delft, Netherlands*

(Received 11 April 2025; revised 27 January 2026; accepted 4 March 2026; published 23 March 2026)

First-order magnetoelastic transitions usually involve mechanisms unique to each family of materials. For $(Mn, Fe)_2(P, Si)$ compounds, it is generally predicted that the unit cell distortion occurring at the ferromagnetic transition leads to a strong electronic reconstruction of the Fe d states accompanied by a notable change in magnetic moment. However, there is no experimental consensus on this mechanism. Here, we use x-ray emission spectroscopy (XES) complemented by first-principles calculations, high-energy resolution fluorescence detected x-ray absorption (HERFD-XAS), and resonant inelastic x-ray scattering (RIXS) experiments, to clarify the nature of the first-order transition in a $Mn_{0.74}Fe_{1.23}P_{0.71}Si_{0.32}$ crystal. HERFD-XAS and RIXS data show a minor evolution of the spectral features in the upper part of the K-edge for Mn and Fe, consistent with the calculated $4p$ density of states and fingerprinting the transition. In contrast, no significant evolution of the XES spectra is observed when the transition is crossed. In Fe-rich compositions, the calculations indicate that Fe at the $3g$ site develops a magnetic moment (2.43 μ_B) that is smaller than that of Mn at the $3g$ site (2.93 μ_B), but larger than that of Fe at the $3f$ site (1.48 μ_B). Quantitative XES analysis using the IAD method gives a reasonable agreement with the magnetic moments for different $(Mn, Fe)_2(P, Si)$ compositions. However, the reduction of the Fe moment predicted by theory (approx. $-0.6\,\mu_B$) is not observed around the transition. This study indicates that the Fe moment collapse at the transition may be weaker than the theoretically predicted value or more gradual in temperature, suggesting a secondary role for this moment instability in the giant magnetocaloric effect of $(Mn, Fe)_2(P, Si)$ compounds.

DOI: 10.1103/dzwg-bnpp

I. INTRODUCTION

Magnetic transitions are most often of the second order type in the Ehrenfest classification. Yet, materials with a first-order magnetic transition (FOMT) are of a strong interest for their ability to realize large changes in properties such as magnetization, volume, entropy, or electrical conduction within a narrow temperature range, leading in turn to the giant effects that form the basis of their applications. Coupling a change in crystal structure with a magnetic transition to form a magneto structural transition is one of the approaches leading to a FOMT. Alternatively, a few materials undergo a FOMT without a change in crystal structure. These isostructural FOMTs are scarcer, especially those that can be induced by temperature or magnetic field at ambient pressure. In this latter case, the coupling mechanism that turns a regular second-order magnetic transition (SOMT) into an isostructural FOMT is more subtle. The origin of these isostructural FOMTs is challenging to establish, as they involve intricated changes in lattice, electronic and magnetic properties. The archetypal example is the antiferromagnetic-to-ferromagnetic isostructural FOMT in FeRh, which has attracted continuous interest over more than 70 years for its coupled volume change, evolution of electronic states and metastability of the Rh magnetic moments [1–4].

Ferromagnetic $La(Fe, Si)_{13}$ and $(Mn, Fe)_2(P, Si)$ materials are more modern examples of isostructural FOMTs, which have recently attracted a dedicated attention, since they present significant advantages for applications, especially those based on their giant magnetocaloric effect [5–13]. In $La(Fe,Si)_{13}$ alloys, the ferromagnetic isostructural FOMT is associated with a large isotropic volume change and is usually described in terms of an itinerant electron metamagnetism mechanism involving a reconstruction of the electronic density of states and a reduction of the average Fe spin moment (from 2.2 μ_B/Fe in the ferromagnetic state to 1.7 μ_B/Fe in the paramagnetic state) [10,14–17]. In contrast, the isostructural FOMT in $(Mn, Fe)_2(P, Si)$ and related Fe_2P compounds shows a nearly negligible volume change, yet it involves a large anisotropic deformation of the hexagonal unit cell. So far, the prevailing model for the FOMT in Fe_2P-based compounds assumes a cooperative mechanism with a lattice deformation, changes in the electronic structure, and a

*Contact author: francois.guillou@unicaen.fr

 ©2026 American Physical Society

metastability of the magnetic moments [12]. However, while a general consensus has been reached on the structural aspects, debates persist on the nature of the electronic reconstructions and on the evolution of the magnetic moments across the FOMT.

$(Mn, Fe)_2(P, Si)$ compounds belong to a broader materials family derived from the Fe_2P parent, including $(Mn, Fe)_2(P, As)$ and $(Mn, Fe)_2(P, Ge)$, which present an exceptional tunability. Chemical compounding not only allows to control their magnetism and adjustment of their Curie temperature over a broad temperature window, but also enables tuning of the strength of the FOMT from a minute latent heat and thermal hysteresis in the binary parent Fe_2P up to a giant FOMT with colossal thermal hysteresis in $MnFeP_{2/3}Si_{1/3}$ [12,18,19]. $(Mn, Fe)_2(P, Si)$ compounds crystallize into the hexagonal Fe_2P-type ($P\bar{6}2m$) structure with Mn and Fe preferably occupying the $3g$ and $3f$ Wyckoff positions, respectively, forming layers that are stacked along the c axis. The metalloid elements substituting phosphorous in the $2c$ and $1b$ sites may also develop a preferential occupancy, for instance Si on the $2c$ site at the highest Si content [20–22]. Upon heating, the ferromagnetic FOMT is accompanied by an expansion of the c axis ($\Delta c/c \approx +4.9\%$) and a contraction of the a axis ($\Delta a/a \approx -2.5\%$), resulting in a nearly negligible volume change ($\Delta V/V \approx -0.02\%$), but a large $\Delta(c/a)/(c/a) \approx 7.5\%$ for the most extreme $MnFeP_{2/3}Si_{1/3}$ compound. This lattice deformation can vary greatly with the strength of the FOMT for different substitutions [19]. The increase in c/a ratio results in increased $3f$-$3g$ interlayer distances, reduced magnetic interactions, and is predicted to induce a strong reconstruction of the electronic states with a reduction in the magnetic moment on the $3f$ site [12].

In the low-temperature ferromagnetic state, for equiatomic MnFe(P,Si) or Mn-rich (Mn,Fe)2(P,Si), neutron powder diffraction, x-ray magnetic circular dichroism (XMCD) and Mössbauer spectroscopy, as well as theoretical calculations, all agree that the $3g$ Mn site carries a large magnetic moment of about 2.9 μ_B/Mn, while the magnetic moment of the $3f$ Fe site is about 1.5 μ_B/Fe. However, controversies have arisen regarding the moment evolution with temperature, in particular when the Curie temperature is crossed. *Ab initio* calculations predict a strong reduction, or even a complete quenching of the magnetic moment on the $3f$ site (more details in Sec. IV) [12]. The development of a spinless state on the $3f$ site has been observed by ^{55}Mn NMR, but spread over a temperature range much larger than the FOMT [23]. In contrast, XMCD measurements in finite applied magnetic fields at the Fe and Mn $L_{2,3}$ edges ($2p \rightarrow 3d$) did not reveal an extinction of the magnetic moment within a limited temperature range around the transition ($T_C \pm 30$ K) [24].

Another issue closely related to the evolution of the moments is that of the electronic structure. Initially, the metastability of the Fe moment was ascribed to a redistribution of the electron density around Fe occupying the $3f$ site concomitant with the structural deformation and filling of the minority band [12]. Experimentally, the formation of more covalent-like bonds between Fe and P/Si atoms has been detected from radial electron density plots obtained from EXAFS and XRD data [25]. X-ray absorption spectroscopy (XAS) at the P K edge ($1s \rightarrow 3p$) has been found to be strongly modified across the FOMT, which offers another fingerprint for the changes in the metal-metalloid bonding at the transition [26]. On the other hand, no clear signature for an evolution of the electronic structure was detected on XAS spectra at L or K edges of Fe or Mn [24,26].

In this work, we use high-energy resolution fluorescence-detected x-ray absorption spectroscopy near-edge structure (HERFD-XAS), $1s3p$ resonant inelastic x-ray scattering (RIXS), and x-ray emission spectroscopy (XES) to probe the evolution of the electronic structure and magnetic moments across the transition. The HERFD-XAS technique is complementary to conventional XAS measurements, as it generally yields comparable absorption spectra while potentially offering advantages in terms of background rejection and reduced spectral broadening [27–29]. The RIXS plane can, in certain cases, provide improved resolution for specific spectral features or reveal electronic excitations that are not accessible through conventional absorption spectroscopy [30–32]. Although multiplet splitting, charge-transfer satellites, or crystal-field fingerprints revealed by RIXS are generally associated with pre-edge excitations and are not expected to be prominent in the present metallic system, this possibility was nevertheless examined.

Most importantly, XES is particularly well suited to address the issue of the evolution of magnetic moments at the FOMT in $(Mn, Fe)_2(P, Si)$, since it is a bulk sensitive method able to track the evolution of the local magnetic moments independently for Fe and Mn, regardless of the presence of a long-range ferromagnetic order, and without applying a magnetic field. The quantitative analysis of $K\beta$ fluorescence lines is nowadays a relatively well-established technique with a demonstrated ability to resolve spin states of transition metals [33,34]. Mainly applied to covalent or ionic compounds, XES has also been shown to be highly useful to address the evolution of the local magnetic moments in metals or intermetallic compounds, including as a function of external driving parameters (temperature or pressure); for instance, in Fe metal [35,36], Invar alloys [37], Fe compounds [38], Heusler alloys [39], carbides [40], phosphides [41] or metallic glasses [42].

In addition to the limitations of each experimental technique, former investigations addressing the FOMT mechanism were often made challenging by a few percents of cubic $(Mn,Fe)_3Si$ ferromagnetic secondary phase in polycrystalline samples and the need to use quenching techniques to avoid their formation [43]. Single crystals are therefore desirable; yet the poor solubility of Si in the flux makes it difficult to grow ferromagnetic crystals, and they usually present an embrittlement when cycled across the FOMT. These issues have recently been overcome by turning to the iron-rich side of the $(Mn, Fe)_2(P, Si)$ phase diagram, for which, compared to the equiatomic $MnFeP_{2/3}Si_{1/3}$, the iron excess increases the Curie temperature near room temperature and weakens the transition (less hysteresis, smaller deformation, better stability upon cycling) [44]. Actually, while the initial investigations on $(Mn, Fe)_2(P, Si)$ compounds for applications were mostly focused on the Mn-rich side of the phase diagram, attention is currently paid to optimizing Fe-rich polycrystalline materials [45–47]. The case of Fe-rich $(Mn, Fe)_2(P, Si)$ single crystals is therefore highly relevant for addressing the FOMT

mechanism responsible for the giant magnetocaloric and thermomagnetic effects in this material family.

As Fe-rich $(Mn, Fe)_2(P, Si)$ compounds have only recently attracted dedicated attention, no complete predictions for the magnetic moments for Fe and Mn in the different metallic positions could be found. Therefore, we first carried out first-principles calculations for a composition reasonably close to that of the investigated single-crystal sample. Then, x-ray spectroscopy experiments are presented for a $Mn_{0.74}Fe_{1.23}P_{0.71}Si_{0.32}$ single crystal. For quantitative analysis, several polycrystalline materials were also investigated [Fe_2P binary parent, $MnFe_{0.95}P_{2/3}Si_{1/3}$, Mn-rich $Mn_{1.28}Fe_{0.67}P_{0.5}Si_{0.5}$, and (Sc,Ti)$Fe_2$ Laves phases]. Only essential information is provided in the main text for these reference materials and more details can be found in the Supplemental Material [48]. Finally, the discussion compares the experimental results with the literature on the metastability of the magnetic moment at the FOMT of Fe_2P materials.

II. THEORETICAL AND EXPERIMENTAL METHODS

Density functional theory (DFT) calculations were carried out using the projector augmented wave (PAW) method as implemented in the VASP package [49–52]. The generalized gradient approximation as parameterized by Perdew-Burke-Ernzerhof (GGA-PBE) was used to describe the exchange-correlation potential. The structure was relaxed until all forces acting on each atom were less than 0.001 eV/Å. The total energies were converged to 10^{-8} eV. For ferromagnetic calculations, a single cell corresponding to thrice the nominal composition $Fe_{4/3}Mn_{2/3}P_{2/3}Si_{1/3}$ was considered with Fe occupying preferentially the 3*f* sites, Mn occupying preferentially the 3*g* site and one of the 3*g* positions occupied by the Fe excess. Calculations for the paramagnetic state were performed using an antiferromagnetic $2 \times 2 \times 1$ supercell while inverting the magnetic moments for the nearest-neighbor metallic atoms in the *a*-*b* plane. Simulations of the Fe and Mn *K*-edge XANES spectra were carried out using the FDMNES code and the experimental lattice parameters for the ferromagnetic and paramagnetic structures [53]. The spectral simulations were performed using the Green's formalism over an aggregate radius of 6.8 Å (≈110 atoms), with one of the 3*g* sites occupied by Fe. The cutting energy of the convolution was shifted by 1 eV.

A $Mn_{0.74\pm0.02}Fe_{1.23\pm0.02}P_{0.71\pm0.01}Si_{0.32\pm0.02}$ single crystal was grown by tin flux as described in [44]. The crystal morphology (hexagonal prismatic shape with smooth surfaces and sharp edges, approximately 770 μm long and 70 μm apparent diameter) and the nominal composition of the crystal was established using a Hitachi TM3030 Plus Scanning Electron Microscope. Magnetic measurements were carried out in a Quantum Design Versalab cryostat employing a vibrating sample magnetometer (VSM) option by mounting the crystal with GE varnish on a quartz paddle. The magnetization measurements were carried out after the x-ray absorption/emission experiments.

$MnFe_{0.95}P_{0.66}Si_{0.34}$, $Mn_{1.28}Fe_{0.67}P_{0.5}Si_{0.5}$, and Fe_2P polycrystalline reference materials were prepared by ball-milling elemental precursors for 10 h in a planetary ball mill, followed by shaping into pellets, sealing into quartz ampules backfilled with a 200 mbar partial pressure of Ar, and performing a solid-state reaction at 1100 °C followed by quenching. Commercial Fe powder from Alfa Aesar was used for metal Fe reference. A bulk polycrystalline reference sample of $Sc_{0.28}Ti_{0.72}Fe_2$ was prepared by arc-melting elemental bulk metals in a purified Ar atmosphere. The button is melted, stirred, and flipped five times, and then sintered at 1000 °C in a quartz ampule backfilled with a 200 mbar partial pressure of Ar, and finally quenched in water at room temperature. Powder x-ray diffraction was carried out at room temperature on an Empyrean Panalytical diffractometer to confirm that the polycrystalline materials had the targeted crystal structures, lattice parameters close to those reported in the literature, and only modest secondary-phase contamination (primary-phase content ⩾95 wt.%).

X-ray absorption and emission experiments were carried out at the ID26 beamline of the European Synchrotron Radiation Facility (ESRF) [28,32]. The sample temperature was controlled by a cold finger cryostat with Kapton windows ensuring high vacuum conditions at the sample space while allowing optical access for x-rays. The single crystal was mounted using double-sided carbon tape. The polycrystalline references were ground into powder, mixed with BN (sample:BN mass ratio 2:1), and pressed into pellets. Only one undulator was used to produce the incident beam, which was monochromatized using a pair of cryogenically cooled Si(111) crystals. Nonresonant Kβ XES spectra were recorded with an incident energy of 7100 eV and 7800 eV for Mn and Fe, respectively, and using a step size of 0.2 eV. Three Ge(620) and two Ge(440) crystal analyzers were used for emission measurements at Fe and Mn edges, respectively. HERFD-XAS spectra were systematically recorded in the same temperature conditions as the XES spectra, by setting the emission energy to 7058.2 eV and 6490.4 eV for Fe and Mn, respectively. At each temperature, ten HERFD-XAS spectra were consecutively recorded, the final spectrum was obtained as their average. RIXS planes were recorded as a sequence of single XAS spectra by scanning the incident energy at successively incremented emission energies. The recorded intensity is plotted on a two-dimensional heat map as a function of energy transfer *vs* incident energy [28,32,54]. The integrals of the absolute values of the difference spectra method (IAD) was used for quantitative interpretation of the nonresonant Kβ data [33,34]. The spectra were interpolated in 0.2 eV increments from 6465 to 6500 eV and from 7035 to 7067 eV for Mn and Fe, respectively, and integrated to unit area. Two XES spectra were successively measured in the same experimental conditions for each element, the final XES is taken as their average and the uncertainty estimated from their difference.

III. RESULTS

A. Electronic structure calculations for Fe-rich $Fe_{4/3}Mn_{2/3}P_{2/3}Si_{1/3}$

First-principles calculations were carried out on $Fe_{4/3}Mn_{2/3}P_{2/3}Si_{1/3}$ using methods comparable to those used for the investigation of equiatomic $MnFeP_{1/2}Si_{1/2}$ compounds [12]. Table I summarizes the relaxed crystal

TABLE I. Unit-cell volume (V), ratio of the lattice parameters (c/a), and magnetic moments per atom for Fe or Mn in the different positions (noted for instance $M_{\mathrm{Fe}-3f}$) in ferromagnetic (FM) and paramagnetic (PM) states for $Fe_{4/3}Mn_{2/3}P_{2/3}Si_{1/3}$.

$Fe_{4/3}Mn_{2/3}P_{2/3}Si_{1/3}$	V (Å^3)	c/a	$M_{\mathrm{Fe}-3f}$ (μ_B/Fe)	$M_{\mathrm{Fe}-3g}$ (μ_B/Fe)	$M_{\mathrm{Mn}-3g}$ (μ_B/Mn)
FM	108.5	0.544	1.477	2.430	2.933
PM	108.7	0.608	0.866	2.074	2.988

structure and magnetic moments in the ferromagnetic (FM) and paramagnetic (PM) states. The relaxed unit-cell volume and c/a ratio of the cell parameters are well in line with a volume-preserving but lattice-deforming FOMT, since from the FM to PM state, the unit-cell difference is negligibly small with $\Delta V/V \approx +0.2\%$, while $\Delta(c/a)/(c/a) \approx 11\%$ is particularly large. Regarding the ferromagnetic moments, the present calculations are well in line with common results for $(Mn, Fe)_2(P, Si)$ compounds. Mn atoms in $3g$ position carry a strong magnetic moment of about 2.9 μ_B/Mn while Fe in $3f$ site shows a smaller moment close to 1.5 μ_B/Fe. More specific to the case of Fe-rich $(Mn, Fe)_2(P, Si)$, the magnetic moment for Fe in $3g$ site, 2.4 μ_B/Fe, is found to be larger than that of Fe in $3f$ site. Predicting a larger moment for Fe in $3g$ site than in the $3f$ site for $Fe_{4/3}Mn_{2/3}P_{2/3}Si_{1/3}$ is consistent with observations made on the Fe_2P binary compound (1.74 and 1.14 μ_B/Fe from Mössbauer [55] and 1.92 and 1.70 μ_B/Fe from polarized neutron diffraction [56]). In the paramagnetic state, the large lattice distortion goes along with a strong redistribution of the metal $3d$ states, affecting the magnetic moments. Quantitatively, the evolution is most pronounced on the Fe $3f$ site with a 0.6 μ_B/Fe decrease in moment. On the $3g$ site, the evolution appears more limited with a 0.35 μ_B decrease for the Fe moment, while the Mn moment experiences a slight increase of 0.05 μ_B. Figure 1 presents projected electronic-structure calculations for p and d states of Mn and Fe atoms in $Fe_{4/3}Mn_{2/3}P_{2/3}Si_{1/3}$. In the ferromagnetic state, one observes significantly sharper main features and a larger exchange splitting for the d states of Mn

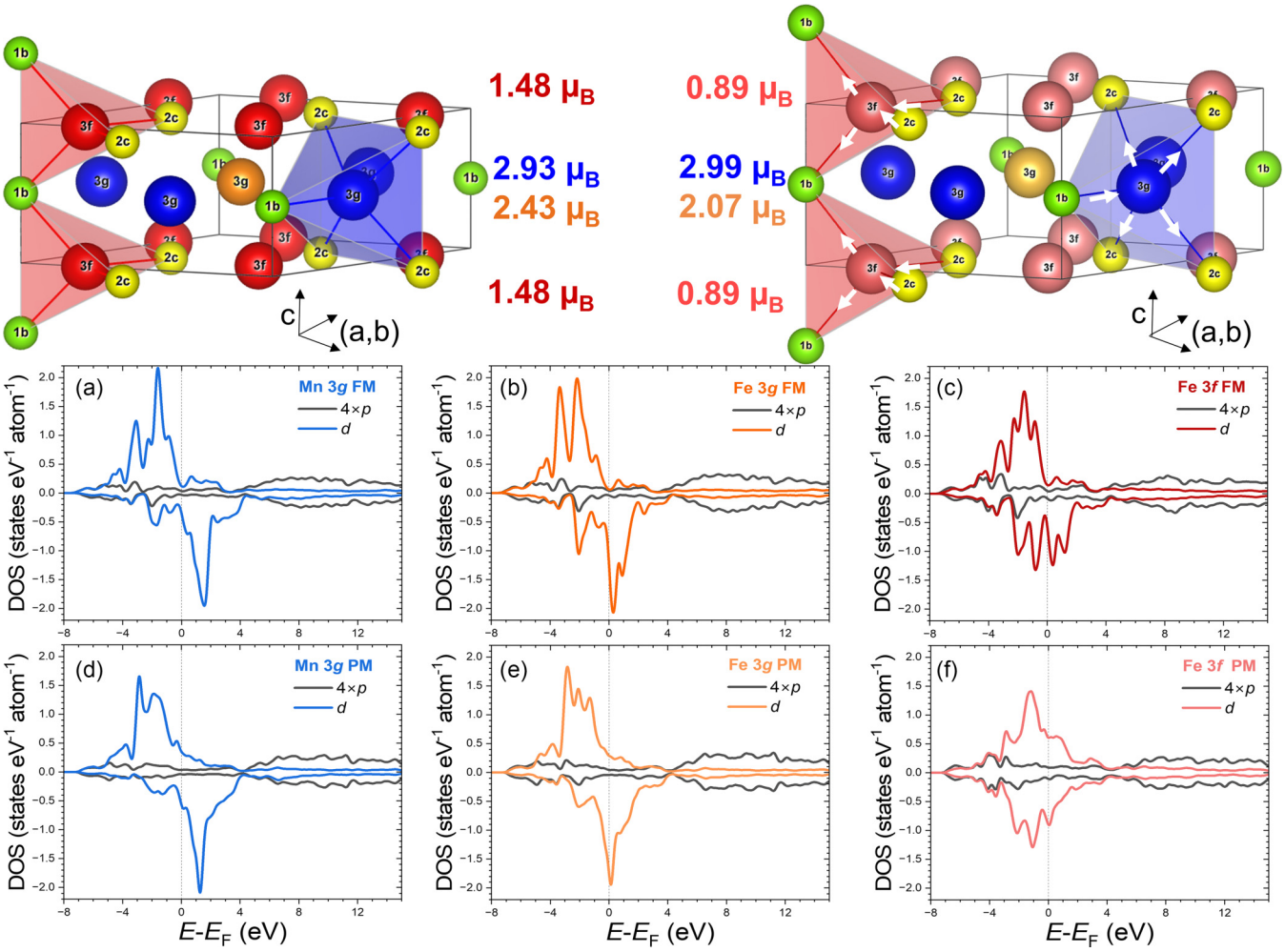

FIG. 1. Schematic representation of the $Fe_{4/3}Mn_{2/3}P_{2/3}Si_{1/3}$ ferromagnetic (left) and paramagnetic (right) unit cells. The polygons highlight the inequivalence between Fe $3f$ sites in a tetrahedron environment of P/Si atoms occupying $2c$ and $1b$ positions and the square-based pyramidal $3g$ sites occupied by Mn and Fe. The arrows mark the evolution of the metal-metalloids distances across the transition. Projected electronic density of states (DOS) in ferromagnetic (a)–(c) and paramagnetic (d)–(f) states. A scalling factor is applied to the p states for visibility.

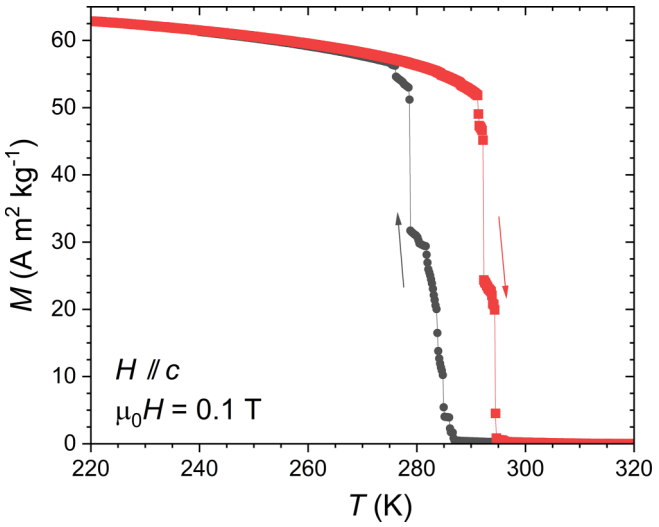

FIG. 2. Magnetization of $Mn_{0.74}Fe_{1.23}P_{0.71}Si_{0.32}$ single crystal in $\mu_0 H = 0.1$ T, upon cooling (circles) and heating (squares).

at the $3g$ site than that for Fe at the $3f$ site, which is primarily responsible for the nearly twice-larger magnetic moment on Mn-$3g$ than Fe-$3f$. The DOS for Fe at the $3g$ site bear more resemblance with that of Mn at the $3g$ site rather than Fe at the $3f$ site, but the extra electron compared to Mn yields a larger occupation of the minority spin channel leading in turn to smaller magnetic moments.

One unit cell of the supercell representative of the paramagnetic state was selected to compare moments and DOS with the FM case. The large deformation of the unit cell leads to significant changes in the d states of Mn and Fe at both the $3f$ and $3g$ sites, but the spin up and down channels become notably more symmetric only for Fe in $3f$ position. A limited, yet present, p-d overlap in the valence band leads to minor DOS features in the p states around –4 eV. Above E_F, the $4p$ states of the metals form two structures with a small contribution from 0 to +3 eV and a broader and denser contribution centered around +8 eV. The evolution across the ferromagnetic transition is relatively subtle for the p states of the metallic atoms compared with those occurring on the d states. In the unoccupied part, the substructures of the broad feature at +8 eV appear to evolve in intensity and position, but these evolutions remain relatively minor.

B. Magnetic and spectroscopy data for $Mn_{0.74}Fe_{1.23}P_{0.71}Si_{0.32}$ single crystal

Figure 2 shows the temperature dependent magnetization of the $Mn_{0.74}Fe_{1.23}P_{0.71}Si_{0.32}$ single crystal. A sharp drop in magnetization marks the ferromagnetic transition centered at 290 K upon heating. A sizable thermal hysteresis of about 12 K is observed upon cooling, confirming the first-order character of this magnetic transition. The transition pathway is somewhat unusual with several discontinuities separated by slowly transforming plateaus. Such burst-like magnetization jumps were previously observed in several $(Mn, Fe)_2(P, Si)$ single crystals and were ascribed to local clamping/release of the strains associated with the ferromagnetic transition and the need to propagate the transition throughout a finite-size crystal [44].

Figure 3 presents the temperature-dependent HERFD-XAS and XES spectra at the Fe and Mn K edges. If one neglects quadrupolar transitions from $1s \rightarrow 3d$ states, K-edge XAS spectra primarily reflect the excitation of a $1s$ electron to unoccupied $4p$ states. In line with former XAS investigations, the Mn and Fe edges are rather metallic in nature, with a broad shoulder in the rising part of the edge, no discernible pre-edge feature, and an upper part of the edge formed by a relatively sharp spectral feature in the FM state. The post-edge region differs markedly between Mn and Fe. Mn exhibits a single broad main structure, whereas Fe shows two distinct features. These differences can be related to the preferential occupancy of Mn on the pyramidal $3g$ site and Fe on the tetrahedral $3f$ site. The single crystal exhibits a Fe-rich composition, resulting in a partial occupation of the $3g$ sites by Fe; consequently, the Fe spectra arise from a dominant contribution of the $3f$ site and a minor contribution from the $3g$ site. XAS spectral simulations were performed assuming a full occupation of Fe on the $3f$ site and a mixed Mn/Fe occupancy on the $3g$ site (separate contributions presented in the Supplemental Material [48]). One can notice a very satisfactory agreement between the experimental and simulated spectra.

Former studies using transmission [25] or total fluorescence-yield [26] detection reported spectral changes upon crossing the transition that were most pronounced in the EXAFS oscillations and showed hardly any modification in the near-edge region. Consistently, the present temperature-dependent measurements show only very limited temperature evolution and therefore agree well with these earlier reports. Nevertheless, a minor yet clearly distinguishable spectral change can be observed upon heating, located at approximately +5 eV relative to the edge midpoint. The associated broadening of this feature is more pronounced toward lower energies for Fe, while it extends toward higher energies for Mn. Reconsidering earlier investigations in light of the present results, we note that a difference between ferromagnetic and paramagnetic states was already present in this energy range in the total fluorescence yield spectra of Ref. [26], albeit much less visible. The evolution of this spectral feature, also expected from simulations, mainly occurs between 270 and 280 K and and therefore confirms that the FOMT is crossed within this temperature interval. The discrepancy in transition temperatures between Figs. 2 and 3 is likely caused by differences in thermometry calibration, as well as by local beam heating during the spectroscopy experiments, both of which may lead to an underestimation of the actual transition temperature. In line with the DOS calculations shown in Fig. 2 and the simulations presented in Fig. 3, the HERFD-XAS data support that the structural distortion occurring at the FOMT affects the unoccupied metal $4p$ states only weakly. By contrast, changes in metal–metalloid distances give rise to more pronounced spectral evolutions at the phosphorous K edge [26].

Figures 3(c) and 3(f) present the Fe and Mn $K\beta$ XES spectra, respectively. For each element, the energy range encompasses the strong $K\beta_{1,3}$ line and the weakest $K\beta$' feature located at lower energies. $K\beta$ fluorescence originates from the transition of a $3p$ electron to a $1s$ hole; while several

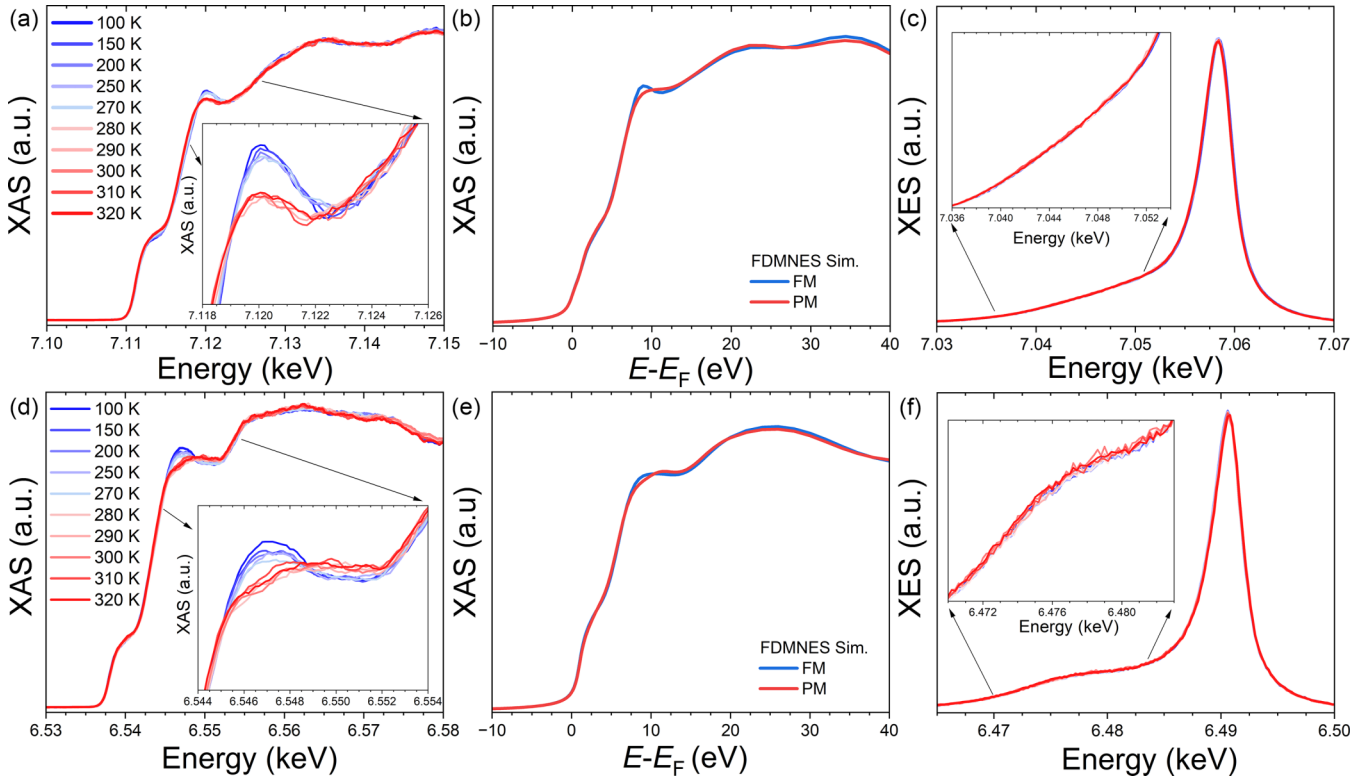

FIG. 3. Temperature dependence of the experimental HERFD-XAS (a),(d) and XES (c),(f) spectra at Fe (top) and Mn (bottom) edges for $Mn_{0.74}Fe_{1.23}P_{0.71}Si_{0.32}$ crystal and FDMNES XAS simulations (b),(e).

mechanisms influence the shape of the fluorescence line, $3p$-$3d$ exchange interaction is usually considered primarily responsible for the splitting between $K\beta_{1,3}$ and $K\beta'$ lines. The presence of a magnetic moment on the $3d$ states is one of the main factors influencing the intensity of $K\beta'$ and the energy splitting between $K\beta_{1,3}$ and $K\beta'$. Here, both the Fe and Mn XES spectra present a relatively broad $K\beta'$ bump typical of metallic compounds. However, one observes that the $K\beta'$ feature is more intense and well separated from $K\beta_{1,3}$ for Mn than for Fe, which is in line with the significantly higher moment predicted for Mn at the $3g$ site than for Fe at $3f$ or $3g$ sites. Most importantly, and in contrast to the XAS spectra recorded under identical conditions, no significant evolution of the XES spectra could be distinguished as a function of temperature. This provides a first qualitative indication that the FOMT in $(Mn, Fe)_2(P, Si)$ does not involve a significant evolution of Mn and Fe magnetic moments.

Figure 4 presents the $1s3p$ RIXS planes recorded in the FM and PM states for Fe and Mn. The RIXS intensity maps are dominated by a strong diagonal feature that closely resembles the HERFD-XAS spectra shown in Fig. 3. In the ferromagnetic state, the upper part of the absorption edge appears slightly more intense than in the PM state, in qualitative agreement with the behavior observed in Fig. 3. A detailed inspection of the $1s3p$ RIXS planes does not reveal other pronounced or independent spectral changes upon increasing temperature. Constant incident energy (CIE) cuts taken at incident energies corresponding to the spectral changes identified in the HERFD-XAS data are dominated by a single asymmetric peak, with an additional broad shoulder observed for Mn. Upon crossing the transition, the peak maxima decrease in intensity, compensated by a broadening of the main peak for Mn, with an additional weak kink emerging at approximately +4 eV relative to the main peak for Fe. The spectral evolutions can be primarily attributed to the same mechanisms that give rise to the differences in XAS. Overall, this initial exploration of the RIXS planes is consistent with XAS studies, indicating only subtle temperature-induced changes for both Fe and Mn.

C. Quantitative XES analysis

To extract more quantitative information from the XES spectra, the integrated average difference method (IAD) has been used with Mn metal and (Sc,Ti)Fe_2 at 250 K as reference spectra for Mn and Fe, respectively. The expected magnetic moments of the references being nonzero, this approach yields only a relative IAD scaling. Table II summarizes the moments, predicted by first-principles calculations or experimentally measured, for the various Mn and Fe compounds. Figure 5 presents the IAD temperature evolution for Mn and Fe in the $Mn_{0.74}Fe_{1.23}P_{0.71}Si_{0.32}$ single crystal and its comparison with the compounds from Table II. For Mn, the IAD of the $Mn_{0.74}Fe_{1.23}P_{0.71}Si_{0.32}$ single crystal is on par with that of $MnFe_{0.95}P_{2/3}Si_{1/3}$. This is well in line with the anticipated similar moments as Mn only occupies the $3g$ site. In comparison, the Mn-rich compound shows a significantly smaller IAD because of the smaller moment of Mn when it occupies the $3f$ site. For Fe, the IAD of the single crystal is slightly lower, but not significantly different from that of $MnFe_{0.95}P_{2/3}Si_{1/3}$,

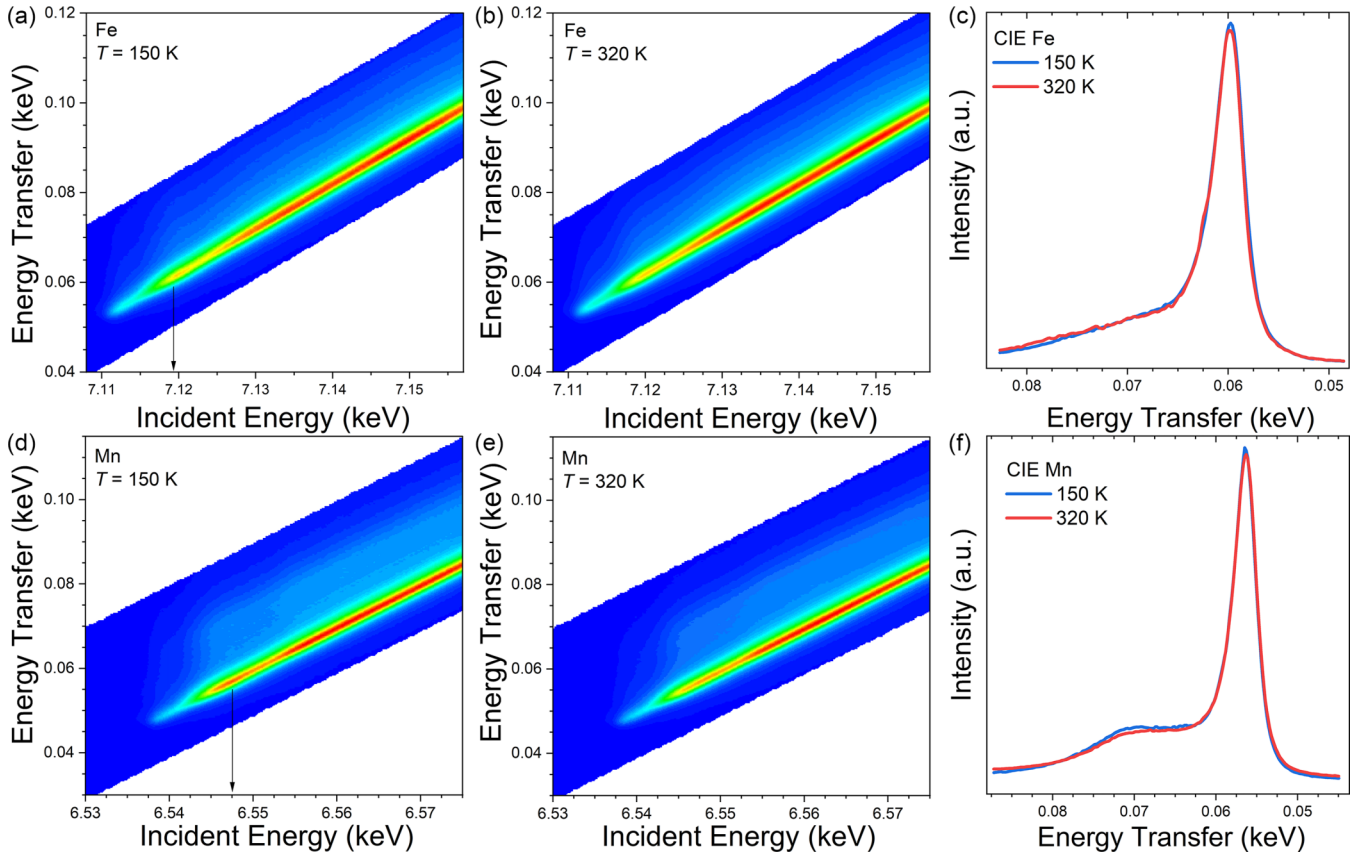

FIG. 4. $1s3p$ RIXS planes for $Mn_{0.74}Fe_{1.23}P_{0.71}Si_{0.32}$ single crystal for Fe (top panels) and Mn (bottom panels) in the ferromagnetic and paramagnetic states (warmer colors corresponding to higher intensities). The arrows indicate the energy location where constant incident energy (CIE) cuts were carried out. The CIE curves were normalized per unit area.

whereas a slightly larger average moment of 1.66 μ_B/Fe was expected for the former, owing to a partial occupation of Fe at the high-moment $3g$ site. This minor inconsistency highlights the limitation of the technique to resolve a limited moment difference. The Si-doped samples show significantly larger Fe moments than the Fe_2P binary parent compound or the Laves phase used as references. Fe metal appears not well aligned in the present IAD scaling. We suspect that the fine Fe powder used for the measurement contains an amorphous fraction with reduced magnetism (the measured magnetization is lower than the expected 2.2 μ_B/Fe), resulting in lower IAD values.

TABLE II. Anticipated magnetic moments on Fe and Mn for the considered references. When bulk magnetization data could not be employed, neutron diffraction results or first-principles calculations (at FM ground state) were used to estimate the atomic moments. The quoted uncertainty reflects the scatter among the available data.

Sample	Fe moment (μ_B/Fe)	Mn moment (μ_B/Mn)	Ref.
Mn metal		0.7(1)	[57]
Fe metal	2.2		
Fe_2P	1.5(1)		[55,56,58]
$MnFe_{0.95}P_{2/3}Si_{1/3}$	1.6(1)	2.9(1)	[12,59–61]
$Mn_{1.28}Fe_{0.67}P_{0.5}Si_{0.5}$	1.5(1)	2.4(3)[a]	[20,61]
$Sc_{0.28}Ti_{0.72}Fe_2$ (50 K)	1.2(1)		[62]
$Sc_{0.28}Ti_{0.72}Fe_2$ (250 K)	0.9(1)		

[a]$3g$: 2.9 μ_B/Mn; $3f$: 0.7 μ_B/Mn.

In line with the close overlap of the $K\beta$ XES spectra from Fig. 3, hardly any significant temperature evolution of the IAD could be distinguished, neither for Mn nor for Fe in the investigated temperature range. A slight increase of the IAD is nevertheless observed for Fe between 100 and 250 K. This evolution remains very limited in amplitude (ΔIAD $\approx$ 0.01, on par with the estimated IAD uncertainty at a given temperature), occurs well below the FOMT, and is not expected; for instance, temperature-dependent neutron diffraction experiments report constant, or even slightly decreasing, magnetic moments on both $3f$ and $3g$ sites far below the Curie temperature [20]. This small increase in IAD is therefore disregarded at first sight.

Temperature-dependent $K\beta$ XES measurements were also carried out on a pressed powder pellet of polycrystalline $MnFe_{0.95}P_{2/3}Si_{1/3}$ (see the Supplemental Material [48]). Even in the latter equiatomic composition, with a clear site preference of Mn for the $3g$ site and of Fe for the $3f$ site, and corresponding to one of the strongest first-order transitions achievable in the Fe_2P system with the largest structural distortion, no significant evolution of the IAD could be noted for Fe and Mn from 20 to 300 K ($T_C \approx$ 230 K upon heating).

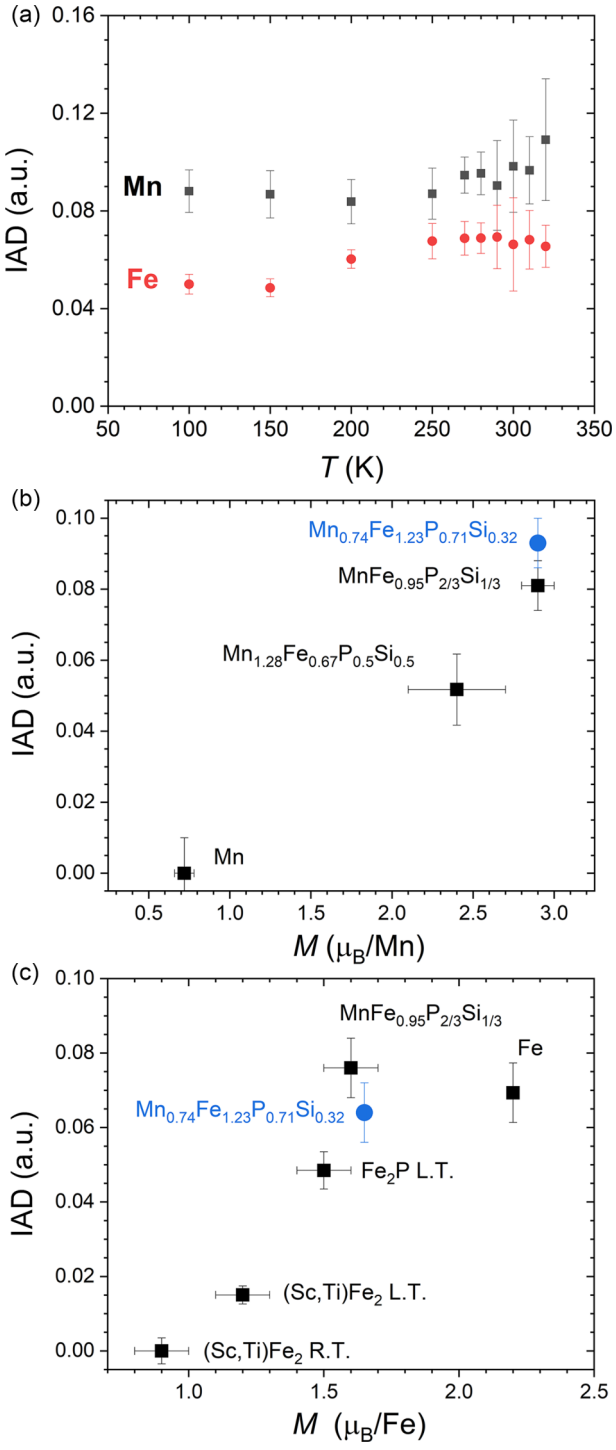

FIG. 5. Quantitative analysis using the integrated absolute difference (IAD) method on XES data. (a) Temperature evolution of the IAD at Fe and Mn edges for the $Mn_{0.74}Fe_{1.23}P_{0.71}Si_{0.32}$ single crystal. (b)(c) IAD as a function of the anticipated magnetic moments (experimental when available, otherwise theoretical) for Mn and Fe, respectively.

IV. DISCUSSION

The presented XES data on a $Mn_{0.74}Fe_{1.23}P_{0.71}Si_{0.32}$ single crystal and its IAD analysis well reflect the expected evolution of the Mn or Fe moments for varying sample compositions, but do not indicate significant changes across the FOMT. The XES method has proven to be a powerful technique to resolve moment collapse induced by a phase transition as a function of the temperature or pressure, such as the one occurring in pnictide superconductors [63,64]. Even if the $K\beta'$ feature is particularly broad in the present metallic (Mn, Fe)$_2$(P, Si) compounds, especially on Fe, a complete moment quenching on the $3f$ site can safely be ruled out in the explored temperature range. The present DFT calculations predicted a decrease of the average moment for Fe from 1.66 μ_B/Fe to 1.10 μ_B/Fe. This moment reduction across the transition is not supported by the present XES data. However, we acknowledge that the accuracy of the IAD technique on the present small single crystal is relatively limited, for instance an expected difference of about 0.2 μ_B/Fe between the $Mn_{0.74}Fe_{1.23}P_{0.71}Si_{0.32}$ crystal and $MnFe_{0.95}P_{2/3}Si_{1/3}$ could not be resolved. A decrease in the $3f$ moment that is more limited than the theoretical prediction, typically a few tenths of Bohr magneton, cannot be discarded experimentally. Several other aspects may also explain the apparent disagreement between theory and experiment.

First, one should recall that the expected amplitude of the moment instability on the $3f$ site presents a relatively large scatter. Table III summarizes most of the quantitative studies on the Fe $3f$ moment instability in Fe_2P compounds. The majority of these investigations have so far been theoretical. The original work highlighting the metamagnetic character of the magnetism in Fe_2P by Yamada and Terao predicted a significant, yet only partial, reduction of the moments on the $3f$ site, from 1.1 to 0.3 μ_B [65]. Subsequent studies confirmed the unstable nature of the magnetism on the $3f$ site in comparison with the more robust $3g$ site. But the actual amplitude of the moment reduction on the $3f$ sites remains controversial; in particular, several works predicted a fully vanishing moment. In quaternary (Mn, Fe)$_2$(P, Si) compounds, similarly to the Fe_2P parent, all theoretical studies suggest a moment instability on the $3f$ site, but of strongly departing intensity. At this stage, the origin for this dispersion in predictions is unclear. The reduction in the Fe $3f$ moment does not correlate with the amplitude of the structural distortions. Therefore, uncertainties in the structural relaxation cannot be identified as the cause. The method used to implement a PM state may have a marked effect. For instance, the supercell approach should, in principle, reflect a paramagnetic disorder. However, it is practically challenging to construct such supercells because of their finite size. The number and arrangement of antiferromagnetically coupled atoms differs in the various studies that employ a supercell approach, influencing the calculated moments in the PM state. On the other hand, disordered local moments calculations consider the existence of magnetic moments in the PM state, albeit fully disordered and collinear. DLM calculations therefore present an alternative to model the PM state, which also indicate a fairly large reduction in $3f$ moments. This suggests that the controversy surrounding the evolution of the $3f$ moments at the FOMT may have a more systematic origin.

The second issue deals with the actual definition of the FM and PM states for a given compound. Most first-principles investigations compare 0 K ground states; whereas, in practice, the transition takes place at finite temperature.

TABLE III. Overview of the former reports quantifying the evolution of the magnetic moment across the FOMT for Fe_2P related compounds. With the exception of an experimental x-ray photoemission spectroscopy study (*), the vast majority of these works are theoretical studies. The method used to model the paramagnetic state is indicated (FerroMagnetic, Fixed-Spin Moment, Disordered Local Moments, antiferromagnetic SuperCell).

	FM			PM					
Material	c/a	$3f$	$3g$	c/a	$3f$	$3g$	$\Delta(c/a)$	Method	Ref.
Fe_2P	0.585	1.08	1.94		0.3	1.5	$\Delta a/a \approx 0.1\%$	FSM	[65]
Fe_2P	0.585	1.02	2.08	0.608	0	1.67	0.023	DLM	[66]
Fe_2P	0.589	0.83	2.30		0.30	2.11		SC	[68]
Fe_2P	0.589	0.95	2.00	0.589	0.06	1.77	0	SC	[68]
Fe_2P		0.85	2.16		≈ 0	1.3		FM	[67]
$MnFeP_{0.5}Si_{0.5}$		1.54	2.8		0.003	2.6		SC	[12]
$MnFeP_{2/3}Si_{1/3}$	0.533	1.45	2.93	0.576	0.67	2.87	0.043	SC	[25]
$MnFeP_{1/3}Si_{2/3}$	0.527	1.509	2.823	0.571	0.695	2.805	0.0441	SC	[61]
$MnFeP_{1/3}Si_{2/3}$	0.499	1.549	2.895	0.569	0.683	2.884	0.07	SC	[61]
$MnFeP_{0.75}Si_{0.25}$	0.535	1.62	2.76	0.592	0.66	2.42	0.057	SC	[60]
$MnFeP_{0.5}Si_{0.5}$	0.5188	1.499	2.854	0.5933	0.795	2.723	0.0745	SC	[69]
$Mn_{1.2}Fe_{0.8}P_{0.5}As_{0.5}$	0.552	1.58	2.85	0.566	≈ 0	2.88	0.014	DLM	[70]
$Mn_{1.1}Fe_{0.9}P_{0.6}As_{0.4}$		1.0	1.26		1.04	1.31		*	[71]

Experimentally, an even more complex aspect is that the transition is not an ideal discontinuity. The purely first-order transition involving the latent heat is spread over a temperature window of a few kelvins. The changes in lattice, electronic, and magnetic properties, however, progressively develop before the transition and keep evolving much after. For instance, in Mn-rich $Mn_{1.25}Fe_{0.70}P_{0.50}Si_{0.50}$, the lattice parameters deviate from a linear evolution about 80 K below the discontinuity at $T_C = 280$ K and become again linear nearly 120 K above it [20]. The paramagnetic susceptibility presents an anomalous behavior over an even broader temperature range. Because of short-range magnetic correlations in the PM regime, a linear Curie-Weiss behavior is reached at temperatures about twice higher than T_C [20,72]. Our present XES investigation was primarily intended to probe the temperature range near the FOMT, where a giant magnetocaloric effect occurs. A zero net magnetization state as modelled by theory may require significantly higher temperatures than presently investigated.

One should finally recall that measuring the magnetic moments in a site-selective or element-selective manner in both the FM and PM states is experimentally challenging as it requires indirect magnetization probes. For instance, in $MnFeP_{1-x}As_x$ compounds, Mössbauer spectroscopy concluded a fairly large reduction of the Fe magnetic moment from 1.1 μ_B to 0.4 μ_B at the magnetoelastic FM-AFM transition for $0.25 \leqslant x \leqslant 0.35$ [73]. On the other hand, neutron diffraction refinements indicated either a strong reduction of the Fe moments from 1.2 μ_B to 0.4(0.1) μ_B or an insignificant difference from 0.9(0.2) μ_B to 0.6(0.25) μ_B, depending on the As content [74]. On a relatively close $Mn_{1.1}Fe_{0.9}P_{0.6}As_{0.4}$ composition, the analysis of photoemission spectra yields nearly identical Fe moments in the FM (1.00 μ_B) and PM (1.04 μ_B) states. Somewhat dissenting observations have also been made in $(Mn,Fe)_2(P,Si)$ compounds. XMCD measurements at the L edges of Fe and Mn did not indicate a complete moment quenching for Fe in the near vicinity of the transition [24]. Neutron diffraction experiments indicated persistent magnetic moment on the $3f$ site in a zero net magnetization state of antiferromagnetic Si-poor $(Mn,Fe)_2(P,Si)$ compounds [75]. No significant evolution of the local magnetic moment is observed at the FOMT on the present XES data. On the other hand, ^{55}Mn NMR spectroscopy observed a spinless state developing on the $3f$ site, but at temperatures well above T_C [23]. Despite the differences, these studies have in common that a complete $3f$ moment collapse was not observed. If present, the $3f$ site moment reduction at the FOMT is likely to fall within the limitations of XES or XMCD methods, i.e., a few tenths of Bohr magneton. A limited $3f$ moment instability is therefore unlikely to be the primary driver of the FOMT, nor the main contributor to the entropy change and giant magnetocaloric effect. In a localized vision of the magnetic entropy in the PM state, $S_{\mathrm{mag}} = k_B \ln(2J+1)$, if only 0.1 electron of spin ½ were involved in the moment instability, it would yield an entropy change $\Delta S_{\mathrm{mag}} \approx 0.1 R \ln 2 \approx 4$ $\mathrm{Jkg^{-1}K^{-1}}$, roughly one order of magnitude smaller than the observed total entropy change in $(Mn,Fe)_2(P,Si)$ materials. This limited contribution aligns with recent studies using inelastic-scattering methods or scaling of physical properties [19,76], which suggest that magnetoelastic deformation may be the primary source of latent heat and entropy change at the FOMT.

V. CONCLUSIONS

X-ray emission spectroscopy (XES), high-energy-resolution x-ray absorption (HERFD-XAS), and resonant inelastic x-ray scattering (RIXS) were measured across the first-order magnetic transition of a $Mn_{0.74}Fe_{1.23}P_{0.71}Si_{0.32}$ single crystal. HERFD-XAS and RIXS data show a minor evolution in the upper part of the K edge for Mn and Fe across the transition, consistent with the relatively mild evolution calculated for the metal $4p$ density of states. In contrast, no significant evolution of the XES spectra is observed when the transition is crossed. Quantitative XES analysis using the IAD method gives reasonable insights into the magnetic moments

for different $(Mn,Fe)_2(P,Si)$ compositions. However, the reduction of the moment on the $3f$ site predicted by theory (approximately –0.6 μ_B) is not observed. The evolution of the Fe moment at the transition is more limited than predicted, suggesting that the moment instability may only be a minor contributor to the entropy change in the giant magnetocaloric effect of $(Mn,Fe)_2(P,Si)$ compounds.

ACKNOWLEDGMENTS

We acknowledge the European Synchrotron Radiation Facility (ESRF) for provision of synchrotron radiation facilities under Proposal No. HC-4931. This work was supported by the National Natural Science Foundation of China (Grants No. 12464015 and No. 52461036) and the program for young talents of science and technology in the Universities of Inner Mongolia autonomous region (Grant No. NJYT23107). The work of F.G. at Caen University was supported by the French government, managed by the Agence Nationale de la Recherche under the France 2030 programme (ANR-23-EXES-0001), by the Normandy region (AIMFER) and a CPJ project.

DATA AVAILABILITY

The data that support the findings of this article are openly available [77], embargo periods may apply.

[1] F. de Bergevin and L. Muldawer, Etude cristallographique de certains alliages de fer rhodium, C. R. Hebd. Séances Acad. Sci. **252**, 1347 (1961).

[2] G. Shirane, R. Nathans, and C. W. Chen, Magnetic moments and unpaired spin densities in the Fe-Rh alloys, Phys. Rev. **134**, A1547 (1964).

[3] A. X. Gray, D. W. Cooke, P. Krüger, C. Bordel, A. M. Kaiser, S. Moyerman, E. E. Fullerton, S. Ueda, Y. Yamashita, A. Gloskovskii, C. M. Schneider, W. Drube, K. Kobayashi, F. Hellman, and C. S. Fadley, Electronic structure changes across the metamagnetic transition in FeRh via hard x-ray photoemission, Phys. Rev. Lett. **108**, 257208 (2012).

[4] L. H. Lewis, C. H. Marrows, and S. Langridge, Coupled magnetic, structural, and electronic phase transitions in FeRh, J. Phys. D: Appl. Phys. **49**, 323002 (2016).

[5] K. A. Gschneidner, Jr., V. K. Pecharsky, and A. O. Tsokol, Recent developments in magnetocaloric materials, Rep. Prog. Phys. **68**, 1479 (2005).

[6] O. Gutfleisch, M. A. Willard, E. Brück, C. H. Chen, S. G. Sankar, and J. Ping Liu, Magnetic materials and devices for the 21st century: Stronger, lighter, and more energy efficient, Adv. Mater. **23**, 821 (2011).

[7] A. Smith, C. R. H. Bahl, R. Bjørk, K. Engelbrecht, K. K. Nielsen, and N. Pryds, Materials challenges for high performance magnetocaloric refrigeration devices, Adv. Energy Mater. **2**, 1288 (2012).

[8] X. Moya, S. Kar-Narayan, and N. D. Mathur, Caloric materials near ferroic phase transitions, Nat. Mater. **13**, 439 (2014).

[9] F. X. Hu, B. G. Shen, J. R. Sun, Z. H. Cheng, G. H. Rao, and X. X. Zhang, Influence of negative lattice expansion and metamagnetic transition on magnetic entropy change in the compound $LaFe_{11.4}Si_{1.6}$, Appl. Phys. Lett. **78**, 3675 (2001).

[10] A. Fujita, S. Fujieda, Y. Hasegawa, and K. Fukamichi, Itinerant-electron metamagnetic transition and large magnetocaloric effects in $La(Fe_xSi_{1-x})_{13}$ compounds and their hydrides, Phys. Rev. B **67**, 104416 (2003).

[11] O. Tegus, E. Brück, K. H. J. Buschow, and F. R. de Boer, Transition-metal based magnetic refrigerants for room-temperature applications, Nature (London) **415**, 150 (2002).

[12] N. H. Dung, Z. Q. Ou, L. Caron, L. Zhang, D. T. Cam Thanh, G. A. de Wijs, R. A. de Groot, K. H. J. Buschow, and E. Brück, Mixed magnetism for refrigeration and energy conversion, Adv. Energy Mater. **1**, 1215 (2011).

[13] F. Guillou, G. Porcari, H. Yibole, N. van Dijk, and E. Brück, Taming the first-order transition in giant magnetocaloric materials, Adv. Mater. **26**, 2671 (2014).

[14] A. Fujita, S. Fujieda, K. Fukamichi, H. Mitamura, and T. Goto, Itinerant-electron metamagnetic transition and large magnetovolume effects in $La(Fe_xSi_{1-x})_{13}$ compounds, Phys. Rev. B **65**, 014410 (2001).

[15] M. E. Gruner, W. Keune, B. Roldan Cuenya, C. Weis, J. Landers, S. I. Makarov, D. Klar, M. Y. Hu, E. E. Alp, J. Zhao, M. Krautz, O. Gutfleisch, and H. Wende, Element-resolved thermodynamics of magnetocaloric $LaFe_{13-x}Si_x$, Phys. Rev. Lett. **114**, 057202 (2015).

[16] E. M. Tapia, C. E. Patrick, T. Hickel, J. Neugebauer, and J. B. Staunton, Quantification of electronic and magnetoelastic mechanisms of first-order magnetic phase transitions from first principles: Application to caloric effects in $La(Fe_xSi_{1-x})_{13}$, J. Phys. Energy **5**, 034004 (2023).

[17] K. P. Skokov, A. Y. Karpenkov, D. Y. Karpenkov, I. A. Radulov, D. Günzing, B. Eggert, A. Rogalev, F. Wilhelm, J. Liu, Y. Shao, *et al.*, A multi-stage, first-order phase transition in $LaFe_{11.8}Si_{1.2}$: Interplay between the structural, magnetic, and electronic degrees of freedom, Appl. Phys. Rev. **10**, 031408 (2023).

[18] M. Hudl, D. Campanini, L. Caron, V. Hoglin, M. Sahlberg, P. Nordblad, and A. Rydh, Thermodynamics around the first-order ferromagnetic phase transition of Fe_2P single crystals, Phys. Rev. B **90**, 144432 (2014).

[19] F. Guillou, H. Yibole, B. Narsu, and V. Hardy, Correlation between deformation and total entropy change at the first-order magnetic transition of Fe_2P-based magnetocaloric materials, Results Phys. **44**, 106203 (2023).

[20] N. H. Dung, L. Zhang, Z. Q. Ou, L. Zhao, L. van Eijck, A. M. Mulders, M. Avdeev, E. Suard, N. H. van Dijk, and E. Brück, High/low-moment phase transition in hexagonal Mn-Fe-P-Si compounds, Phys. Rev. B **86**, 045134 (2012).

[21] X. F. Miao, L. Caron, P. Roy, N. H. Dung, L. Zhang, W. A. Kockelmann, R. A. de Groot, N. H. van Dijk, and E. Brück, Tuning the phase transition in transition-metal-based magnetocaloric compounds, Phys. Rev. B **89**, 174429 (2014).

[22] D. Fruchart, S. Haj-Khlifa, P. de Rango, M. Balli, R. Zach, W. Chajec, P. Fornal, J. Stanek, S. Kaprzyk, and J. Tobola, Structure and magnetic properties of bulk synthesized $Mn_{2-x}Fe_xP_{1-y}Si_y$ compounds from magnetization, ^{57}Fe

Mössbauer spectroscopy, and electronic structure calculations, Crystals **9**, 37 (2019).

[23] R. Hussain, F. Cugini, S. Baldini, G. Porcari, N. Sarzi Amadè, X. F. Miao, N. H. van Dijk, E. Brück, M. Solzi, R. De Renzi, and G. Allodi, Ubiquitous first-order transitions and site-selective vanishing of the magnetic moment in giant magnetocaloric MnFeSiP alloys detected by ^{55}Mn NMR, Phys. Rev. B **100**, 104439 (2019).

[24] H. Yibole, F. Guillou, L. Caron, E. Jiménez, F. M. F. de Groot, P. Roy, R. de Groot, N. H. van Dijk, and E. Brück, Moment evolution across the ferromagnetic phase transition of giant magnetocaloric (Mn, Fe)$_2$(P, Si, B) compounds, Phys. Rev. B **91**, 014429 (2015).

[25] M. F. J. Boeije, P. Roy, F. Guillou, H. Yibole, X. F. Miao, L. Caron, D. Banerjee, N. H. van Dijk, R. A. de Groot, and E. Brück, Efficient room-temperature cooling with magnets, Chem. Mater. **28**, 4901 (2016).

[26] F. Guillou, K. Ollefs, F. Wilhelm, A. Rogalev, A. N. Yaresko, H. Yibole, N. H. van Dijk, and E. Brück, Electronic and magnetic properties of phosphorus across the first-order ferromagnetic transition of (Mn, Fe)$_2$(P, Si, B) giant magnetocaloric materials, Phys. Rev. B **92**, 224427 (2015).

[27] O. V. Safonova, M. Tromp, J. A. van Bokhoven, F. M. F. de Groot, J. Evans, and P. Glatzel, Identification of CO adsorption sites in supported Pt catalysts using high-energy-resolution fluorescence detection x-ray spectroscopy, J. Phys. Chem. B **110**, 16162 (2006).

[28] P. Glatzel, T. C. Weng, K. Kvashnina, J. Swarbrick, M. Sikor, E. Gallo, N. Smolentsev, and R. Alonso Mori, Reflections on hard x-ray photon-in/photon-out spectroscopy for electronic structure studies, J. Electron Spectrosc. Relat. Phenom. **188**, 17 (2013).

[29] M. Bauer, HERFD-XAS and valence-to-core-XES: New tools to push the limits in research with hard x-rays? Phys. Chem. Chem. Phys. **16**, 13827 (2014).

[30] J. Wang, C. S. Hsu, T. S. Wu, T. S. Chan, N. T. Suen, J. F. Lee, and H. M. Chen, In situ x-ray spectroscopies beyond conventional x ray absorption spectroscopy on deciphering dynamic configuration of electrocatalysts, Nat. Commun. **14**, 6576 (2023).

[31] A. Kotani and S. Shin, Resonant inelastic x-ray scattering spectra for electrons in solids, Rev. Mod. Phys. **73**, 203 (2001).

[32] P. Glatzel and U. Bergmann, High resolution 1*s* core hole x-ray spectroscopy in 3*d* transition metal complexes-electronic and structural information, Coord. Chem. Rev. **249**, 65 (2005).

[33] G. Vanko, T. Neisius, G. Molnar, F. Renz, S. Karpati, A. Shukla, and F. M. F. de Groot, Probing the 3*d* spin momentum with x-ray emission spectroscopy: The case of molecular-spin transitions, J. Phys. Chem. B **110**, 11647 (2006).

[34] S. Lafuerza, A. Carlantuono, M. Retegan, and P. Glatzel, Chemical sensitivity of $K\beta$ and $K\alpha$ x-ray emission from a systematic investigation of iron compounds, Inorg. Chem. **59**, 12518 (2020).

[35] J. P. Rueff, M. Krisch, Y. Q. Cai, A. Kaprolat, M. Hanfland, M. Lorenzen, C. Masciovecchio, R. Verbeni, and F. Sette, Magnetic and structural $\alpha - \epsilon$ phase transition in Fe monitored by x-ray emission spectroscopy, Phys. Rev. B **60**, 14510 (1999).

[36] J. P. Rueff, M. Mezouar, and M. Acet, Short-range magnetic collapse of Fe under high pressure at high temperatures observed using x-ray emission spectroscopy, Phys. Rev. B **78**, 100405(R) (2008).

[37] J. P. Rueff, A. Shukla, A. Kaprolat, M. Krisch, M. Lorenzen, F. Sette, and R. Verbeni, Magnetism of Invar alloys under pressure examined by inelastic x-ray scattering, Phys. Rev. B **63**, 132409 (2001).

[38] H. Yamaoka, N. Tsujii, H. Oohashi, D. Nomoto, I. Jarrige, K. Takahiro, K. Ozaki, K. Kawatsura, and Y. Takahashi, Bulk electronic properties of $FeSi_{1-x}Ge_x$ investigated by high-resolution x-ray spectroscopies, Phys. Rev. B **77**, 115201 (2008).

[39] A. Svyazhin, E. Kurmaev, E. Shreder, S. Shamin, and C. J. Sahle, Local moments and electronic correlations in Fe-based Heusler alloys: Kα x-ray emission spectra measurements, J. Alloys Compd. **679**, 268 (2016).

[40] J. F. Lin, V. V. Struzhkin, H. Mao, R. J. Hemley, P. Chow, M. Y. Hu, and J. Li, Magnetic transition in compressed Fe_3C from x-ray emission spectroscopy, Phys. Rev. B **70**, 212405 (2004).

[41] F. Han, D. Wang, Y. Wang, N. Li, J. K. Bao, B. Li, A. S Botana, Y. Xiao, P. Chow, and D. Y. Chung, Spin quenching assisted by a strongly anisotropic compression behavior in MnP, New J. Phys. **20**, 023012 (2018).

[42] T. Liang, F. Zhang, X. Zhang, X. Chen, S. Chen, H. Lou, Z. Zeng, D. Xu, K. Yang, Y. Xiao, P. Chow, B. Shen, and Q. Zeng, Pressure-induced spin crossover in a metallic glass, J. Appl. Phys. **129**, 165901 (2021).

[43] V. Höglin, J. Cedervall, M. S. Andersson, T. Sarkar, M. Hudl, P. Nordblad, Y. Andersson, and M. Sahlberg, Phase diagram, structures and magnetism of the $FeMnP_{1-x}Si_x$-system, RSC Adv. **5**, 8278 (2015).

[44] L. L. Bao, W. Meijuan, H. Yibole, Z. Q. Ou, and F. Guillou, Magnetization steps at the ferromagnetic transition of (Mn, Fe)$_2$(P, Si) single crystals, J. Alloys Compd. **970**, 172612 (2024).

[45] F. Zhang, I. Batashev, Q. Shen, Z. Wu, R. I. Smith, G. A. de Wijs, N. H. van Dijk, and E. Brück, Impact of F and S doping on (Mn, Fe)$_2$(P, Si) giant magnetocaloric materials, Acta Mater. **234**, 118057 (2022).

[46] F. Zhang, I. Batashev, N. H. van Dijk, and E. Brück, Effect of off-stoichiometry and Ta doping on Fe-rich (Mn, Fe)$_2$(P, Si) based giant magnetocaloric materials, Scripta Mater. **226**, 115253 (2023).

[47] S. Ghorai, J. Cedervall, R. Clulow, S. Huang, T. Ericsson, L. Häggström, V. Shtender, E. K. Delczeg-Czirjak, L. Vitos, O. Eriksson, M. Sahlberg, and P. Svedlindh, Site-specific atomic substitution in a giant magnetocaloric Fe_2P-type system, Phys. Rev. B **107**, 104409 (2023).

[48] See Supplemental Material at http://link.aps.org/supplemental/10.1103/dzwg-bnpp for data on reference materials, XAS simulations for non-equivalent sites, and the temperature dependence of the IAD for polycrystalline $MnFe_{0.95}P_{2/3}Si_{1/3}$.

[49] P. Hohenberg and W. Kohn, Inhomogeneous electron gas, Phys. Rev. **136**, B864 (1964).

[50] W. Kohn and L. J. Sham, Self-consistent equations including exchange and correlation effects, Phys. Rev. **140**, A1133 (1965).

[51] G. Kresse and J. Hafner, *Ab initio* molecular dynamics for liquid metals, Phys. Rev. B **47**, 558 (1993).

[52] G. Kresse and J. Furthmüller, Efficient iterative schemes for *ab initio* total-energy calculations using a plane-wave basis set, Phys. Rev. B **54**, 11169 (1996).

[53] O. Bunău and Y. Joly, Self-consistent aspects of x-ray absorption calculations, J. Phys.: Condens. Matter **21**, 345501 (2009).

[54] F. M. F de Groot, M. W. Haverkort, H. Elnaggar, A. Juhin, K. J. Zhou, and P. Glatzel, Resonant inelastic x-ray scattering, Nat. Rev. Methods Primers **4**, 45 (2024).

[55] R. Wäppling, L. Häggström, T. Ericsson, S. Devanarayanan, E. Karlsson, B. Carlsson, and S. Rundqvist, First order magnetic transition, magnetic structure and vacancy distribution in Fe_2P, J. Phys. Colloques **35**, C6-597 (1974).

[56] H. Fujii, S. Komura, T. Takeda, T. Okamoto, Y. Ito, and J. Akimitsu, Polarized neutron diffraction study of Fe_2P single crystal, J. Phys. Soc. Jpn. **46**, 1616 (1979).

[57] D. Hobbs, J. Hafner, and D. Spišák, Understanding the complex metallic element Mn. I. Crystalline and noncollinear magnetic structure of α-Mn, Phys. Rev. B **68**, 014407 (2003).

[58] L. Caron, M. Hudl, V. Höglin, N. H. Dung, C. P. Gomez, M. Sahlberg, E. Brück, Y. Andersson, and P. Nordblad, Magnetocrystalline anisotropy and the magnetocaloric effect in Fe_2P, Phys. Rev. B **88**, 094440 (2013).

[59] Z. Q. Ou, N. H. Dung, L. Zhang, L. Caron, E. Torun, N. H. van Dijk, O. Tegus, and E. Brück, Transition metal substitution in Fe_2P based $MnFe_{0.95}P_{0.50}Si_{0.50}$ magnetocaloric compounds, J. Alloys Compd. **730**, 392 (2018).

[60] G. Li, W. Li, S. Schönecker, X. Li, E. K. Delczeg-Czirjak, Y. O. Kvashnin, O. Eriksson, B. Johansson, and L. Vitos, Kinetic arrest induced antiferromagnetic order in hexagonal $FeMnP_{0.75}Si_{0.25}$ alloy, Appl. Phys. Lett. **105**, 262405 (2014).

[61] P. Roy, E. Torun, and R. A. de Groot, Effect of doping and elastic properties in $(Mn, Fe)_2(Si, P)$, Phys. Rev. B **93**, 094110 (2016).

[62] Y. Nishihara and Y. Yamaguchi, Magnetic properties of the $(Sc_{1-x}Ti_x)Fe_2$ system having two magnetic states with different degrees of localization, J. Phys. Soc. Jpn. **55**, 920 (1986).

[63] H. Gretarsson, A. Lupascu, J. Kim, D. Casa, T. Gog, W. Wu, S. R. Julian, Z. J. Xu, J. S. Wen, G. D. Gu, R. H. Yuan, Z. G. Chen, N. L. Wang, S. Khim, K. H. Kim, M. Ishikado, I. Jarrige, S. Shamoto, J. H. Chu, I. R. Fisher, *et al.*, Revealing the dual nature of magnetism in iron pnictides and iron chalcogenides using x-ray emission spectroscopy, Phys. Rev. B **84**, 100509(R) (2011).

[64] H. Gretarsson, S. R. Saha, T. Drye, J. Paglione, J. Kim, D. Casa, T. Gog, W. Wu, S. R. Julian, and Y. J. Kim, Spin-state transition in the Fe pnictides, Phys. Rev. Lett. **110**, 047003 (2013).

[65] H. Yamada and K. Terao, First-order transition of Fe_2P and antimetamagnetic transition, Ph. Transit. **75**, 231 (2002).

[66] E. K. Delczeg-Czirjak, L. Delczeg, M. P. J. Punkkinen, B. Johansson, O. Eriksson, and L. Vitos, *Ab initio* study of structural and magnetic properties of Si-doped Fe_2P, Phys. Rev. B **82**, 085103 (2010).

[67] Z. Gercsi, E. K. Delczeg-Czirjak, L. Vitos, A. S. Wills, A. Daoud-Aladine, and K. G. Sandeman, Magnetoelastic effects in doped Fe_2P, Phys. Rev. B **88**, 024417 (2013).

[68] X. B. Liu, J. Ping Liu, Q. Zhang, and Z. Altounian, Fe magnetic moment formation and exchange interaction in Fe_2P: A first-principles study, Phys. Lett. A **377**, 731 (2013).

[69] B. Wurentuya, S. Ma, B. Narsu, O. Tegus, and Z. Zhang, Lattice dynamics of $FeMnP_{0.5}Si_{0.5}$ compound from first principles calculation, J. Mater. Sci. Technol. **35**, 127 (2019).

[70] V. I. Val'kov and A. V. Golovchan, Electronic mechanism of spontaneous magnetostriction in the layered system $Mn_{2-x}Fe_xAs_{0.5}P_{0.5}$, Low Temp. Phys. **39**, 701 (2013).

[71] J. Kubacki, K. Balin, M. Kulpa, Ł. Hawełek, P. Włodarczyk, P. Zackiewicz, M. Kowalczyk, M. Polak, and J. Szade, Magnetic moments and exchange splitting in Mn 3*s* and Mn 2*p* core levels of magnetocaloric $Mn_{1.1}Fe_{0.9}P_{0.6}As_{0.4}$ and $Mn_{1.1}Fe_{0.9}P_{0.5}As_{0.4}Si_{0.1}$ compounds, Physica B **549**, 127 (2018).

[72] X. F. Miao, L. Caron, P. C. M. Gubbens, A. Yaouanc, P. Dalmas de Réotier, H. Luetkens, A. Amato, N. H. van Dijk, and E. Brück, Spin correlations in $(Mn, Fe)_2(P, Si)$ magnetocaloric compounds above Curie temperature, J. Sci.: Adv. Mater. Devices **1**, 147 (2016).

[73] M. Bacmann, J. L. Soubeyroux, R. Barrett, D. Fruchart, R. Zach, S. Niziol, and R. Fruchart, Magnetoelastic transition and antiferro-ferromagnetic ordering in the system $MnFeP_{1-y}As_y$, J. Magn. Magn. Mater. **134**, 59 (1994).

[74] B. Malaman, G. Le Caër, P. Delcroix, D. Fruchart, M. Bacmann, and R. Fruchart, Magneto-elastic transition and magnetic couplings: A ^{57}Fe Mössbauer spectroscopy study of the $MnFeP_{1-x}As_x$ system, J. Phys.: Condens. Matter **8**, 8653 (1996).

[75] K. K. Thilakan, S. Ghorai, W. Liu, L. Häggström, F. Lindgren, V. Pomjakushin, P. Beran, O. Gutfleisch, P. Svedlindhgh, and J. Cedervall, Revealing complex magnetic interactions in Fe_2P-based compounds: A study using Mössbauer spectroscopy and neutron diffraction, J. Mater. Chem. A **13**, 30128 (2025).

[76] D. Bessas, M. Maschek, H. Yibole, J. W. Lai, S. M. Souliou, I. Sergueev, A. I. Dugulan, N. H. van Dijk, and E. Brück, Lattice dynamics across the magnetic transition in $(Mn, Fe)_{1.95}(P, Si)$, Phys. Rev. B **97**, 094303 (2018).

[77] H. Yibole, Electronic structure and local moments in single-crystaline MnFe(P,Si) probed by linear dichroic XES and HERFD-XAS [Dataset], European Synchrotron Radiation Facility (2025), https://doi.org/10.15151/ESRF-ES-804828516.